HHS Public Access

Author manuscript

Nature. Author manuscript; available in PMC 2020 January 31.

Published in final edited form as:

Nature. 2019 August ; 572(7768): 244–248. doi:10.1038/s41586-019-1453-3.

Cholera toxin promotes pathogen acquisition of host-derived nutrients

Fabian Rivera-Chávez[1], **John J. Mekalanos**[1,*]

[1]Department of Microbiology and Immunobiology, Harvard Medical School, Boston, MA 02115, USA.

Abstract

Vibrio cholerae is the causative agent of cholera, a potentially lethal enteric bacterial infection[1]. Cholera toxin (CT) is required for *V. cholerae* to cause severe disease and is also thought to promote transmission of the organism in that victims can shed many liters of diarrheal fluid that typically contains in excess of 10^{11} organisms per liter. How the pathogen is able to reach such high concentrations in the intestine during infection remains poorly understood. Here we show that CT-mediated disease enhances pathogen growth and induces a distinct *V. cholerae* transcriptome signature that is indicative an iron-depleted gut niche. During infection, bacterial pathogens need to acquire iron, a nutrient essential for growth[2]. The majority of iron in the mammalian host resides in a chelated form within the porphyrin structure of heme, and *V. cholerae* genetically encodes the ability to utilize heme as a source of iron[3]. We show that *V. cholerae* heme and vibriobactin utilization genes confer a growth advantage to the pathogen only when CT is produced. Furthermore, CT-induced capillary congestion pathology in the terminal ileum correlated with an increased bioavailability of luminal heme. CT-induced disease in the ileum also led to increased luminal concentrations of long-chain fatty acids (LCFAs) and L-lactate metabolites, as well as upregulation of *V. cholerae* iron-sulfur cluster-containing TCA cycle enzyme genes. Genetic analysis of *V. cholerae* suggested that heme and LCFA uptake-dependent growth of *V. cholerae* occurs during infection but only in a strain capable of producing CT *in vivo*. We conclude that CT-induced disease creates an iron-depleted metabolic niche in the gut that selectively promotes the explosive growth of this pathogen through acquisition of host-derived heme and fatty acids as nutrients.

The enterotoxin activity of CT from supernatants of *V. cholerae* cultures was first reported almost 60 years ago[4]. The catalytic activity of CT activates adenylyl cyclase, which increases cellular levels of 3',5'-cyclic AMP (cAMP) leading to changes in numerous metabolic functions regulated by the cAMP-dependent protein kinase PKA[5]. The massive secretory diarrhea caused by CT is thought to occur when PKA phosphorylates and activates

---

*To whom correspondence should be addressed. john_mekalanos@hms.harvard.edu.

Author Contributions. F.R.-C. performed and analyzed the experiments. F.R.-C. and J.J.M. were responsible for the overall study design and for writing the manuscript.

The authors declare no competing financial interests. Readers are welcome to comment on the online version of the paper.

ion channels that ultimate lead to electrolyte imbalances in the intestinal lumen[6]. Elevation of cAMP levels is also able to include lipolysis and indeed CT can cause massive breakdown of lipids in adipose cells[7]. Recent studies have indicated that some virulence factors can promote pathogen acquisition of nutrients in the host gut by generation of inflammation-associated metabolites[8]. Although CT is thought to confer a fitness advantage to *V. cholerae* by increasing the dissemination of the organism during outbreaks, we wondered whether CT stimulates intestinal growth of *V. cholerae* by affecting host metabolism and nutrient acquisition by this pathogen.

To test this hypothesis, we first asked whether CT can enhance the growth of *V. cholerae* during infection of 3-day old neonatal (infant) rabbits because these experimental animals show CT-dependent disease symptoms similar to what is observed during human infection[9]. Rabbit pups were infected with either wild type (WT) *V. cholerae* C6706 or an isogenic in-frame Δ*ctxAB* mutant (FRC38) which is unable to produce either the A or B subunits of CT (from here forward referred to as Δ*ctx*) (Extended Data Fig. 1a). As expected, pups infected with the WT strain but not the Δ*ctx* mutant developed severe diarrheal disease one day after infection (Fig. 1a). Consistent with previous observations, no difference in bacterial concentrations (CFU/g) in the tissue of the ileum (small intestine) or downstream in the fluid of the cecum were observed between infant rabbits infected with either the WT or Δ*ctx* mutant (Fig. 1b and Fig. 1c). However, standard CFU normalization by weight is misleading because the cholera-like disease caused by the WT strain led to massive intestinal fluid accumulation and loss (Fig. 1a). When we corrected for the volume of fluid present in the lumen of the intestinal cecum, we found that the WT *V. cholerae* reached ~22-fold higher levels than the Δ*ctx* mutant in the gut lumen (Fig. 1d). This growth yield difference was not observed when WT was competed with the Δ*ctx* mutant in mixed infections (Extended Data Fig. 1b), suggesting that CT-enhanced colonization depends on secreted CT and its effect on the host intestinal environment.

Previously, RNA-seq transcriptome analysis has been used to correlate changes in *V. cholerae* gene expression with the presence of metabolites in the gut during infection of neonatal rabbits[10]. To understand how CT enhances the replication of this organism within the intestine, strand-specific Illumina-based RNA-seq analysis[11] was performed on two samples each of WT and the Δ*ctx* mutant bacteria harvested from either the rabbit ileum or the cecum one-day post-intragastric infection (Fig. 1e-h). We observed a strong correlation between RNA-seq biological replicates in both the WT and Δ*ctx* mutant samples obtained (Extended Data Fig. 2a-d). Principle coordinate analysis (PCA) revealed that there was a marked difference in gene expression in WT bacteria harvested from the ileum compared to the adjacent cecum (Extended Data Fig. 3a). Although most open reading frames (ORFs) were not differentially expressed, we found 128 genes that were significantly up-regulated in WT *V. cholerae* colonizing the ileum relative to the cecum (Supplementary Table 1) and that these included many virulence genes in the ToxT regulon (Extended Data Fig. 3b). Notably, the ToxT-regulated genes encoding CT (*ctxA* and *ctxB*) were the most highly expressed ORFs in WT bacteria recovered from the ileum.

We next compared gene expression in the WT and Δ*ctx* mutant and found a *V. cholerae* transcriptome signature that correlated with the capacity to produce CT regardless of

anatomical location (Fig. 1e). We found 243 genes that were significantly up-regulated in the WT compared to the Δ*ctx* mutant and these included 101 genes in ileum samples, 118 in the cecum samples, and 24 in both samples (Fig. 1f, Supplementary Table 2). Interestingly, although most ORFs were not differentially expressed in the WT compared to the Δ*ctx* mutant, virulence factors including many encoded by ToxT-regulated genes were up-regulated in the WT cells compared to the Δ*ctx* mutant (Extended Data Fig. 4a and 4b), suggesting that CT induced changes in the gut environment may provide a positive signal for ToxT-regulated virulence gene expression.

The *V. cholerae* genome consists two circular chromosomes: a large (2,961,146 bp) chromosome (Chr. I), and a smaller (1,072,314 bp) chromosome (Chr. II)[12]. Surprisingly, we observed a 16-fold induction in transcription originating from Chr. II in the WT cells relative to the Δ*ctx* mutant during colonization of the ileum (Fig. 1g), and 4-fold induction in the cecum (Extended Data Fig. 4c and 4d). Remarkably, we found that expression of just 10 genes involved in heme utilization accounted for almost 14% of the entire Chr. II transcriptome during colonization of the ileum and that these genes were up-regulated nearly 20-fold in WT compared to the Δ*ctx* mutant (Fig. 1h). Further analysis revealed that virtually all genes involved in heme uptake and vibriobactin-mediated iron acquisition that were located on either Chr. I and Chr. II were highly up-regulated in WT relative to the Δ*ctx* mutant and this induction occurred most prominently in the ileum relative to the cecum (Fig. 2a, Extended Data Fig. 4e, and, Supplementary Table 3).

When iron is a limiting nutrient, *V. cholerae* is capable of expressing multiple iron acquisition systems that include receptors and TonB-dependent transporters of heme as well as the siderophore vibriobactin, its receptor, and transport systems[13], a process that is controlled by the Ferric Uptake Regulator (Fur)[14]. We found that almost all Fur-controlled genes known to be induced under low-iron growth conditions were up-regulated in WT relative to the Δ*ctx* mutant in both the ileum and in the cecum, with a marked up-regulation in the ileum relative to the cecum (Extended Data Fig. 5, Supplementary Table 3). Furthermore, 18 of the 24 genes up-regulated in both the ileum and cecum in WT cells are known to be induced under low iron conditions (Fig. 1f, Supplementary Table 2). We next memeasured the concentration of iron in the ileum of infant rabbits by triple quadrupole ICP-MS (ICP-QQQ-MS). Remarkably, iron levels were significantly reduced in the ileum samples collected from WT infected animals compared to those infected with the Δ*ctx* mutant (Fig. 2b). We wondered if CT was inducing local intestinal inflammation which could deplete available iron via host iron-binding proteins such as neutrophil lactorferrin[15]. However, we found that a stable marker of inflammation, the iron-sequestration protein Lipocalin-2[16] was not elevated in the gut of infant rabbits infected with the WT relative to the Δ*ctx* mutant (Extended Data Fig. 5d).

The presence of free heme has previously been reported in the intestinal lumen of neonatal rabbits infected with *V. cholerae*[9]. Remarkably, rabbits infected with WT *V. cholerae* exhibited elevated concentrations of heme (measured as hemin) in luminal samples from the ileum and the cecum relative to animals infected with the Δ*ctx* mutant (Fig. 2c). Higher concentrations of hemin were detected in the ileum relative to the cecum for WT infected rabbits and these data are consistent with our RNA-seq data that showed higher expression

of heme utilization genes in ileum relative to the cecum (Fig. 2a, Supplementary Table 3). Collectively, these data indicate that infection with *V. cholerae* leads to a CT-mediated increase of heme in the gut lumen.

Infection with *V. cholerae* leads to capillary congestion of red blood cells in the ileum of the small intestine[4,17]. *V. cholerae* studies in neonatal rabbits have demonstrated that capillary congestion requires CT[9]. Neonatal (suckling) mice exhibit CT-dependent diarrheal disease, and are commonly used as a model for evaluating *V. cholerae* mutants for defects in intestinal colonization[18]. Interestingly, heme utilization genes have also been found to be upregulated in the infant mouse gut[10]. To investigate whether CT induces capillary congestion in mice, 4-day old suckling mice were infected with either WT or with the Δ*ctx* mutant, mock infected, or treated with purified CT. While no mice exhibited signs of inflammation (Extended Data Fig. 6a and 6b), infection with the WT or oral treatment with CT resulted in capillary congestion of red blood cells in the small intestine (Extended Data Fig. 6a), which correlated with CT-dependent fluid accumulation and elevated concentrations of heme (Extended Data Fig. 6c and 6d). Interestingly, elevated levels of heme were not detected in the ileum of wild type infected animals, suggesting that heme may be a limiting nutrient in the mouse gut (Extended Data Fig. 6d).

We next determined whether CT could also enhance growth of *V. cholerae* in the mouse gut. We observed significantly higher total bacterial numbers in the GI tracts of WT infected mice compared to Δ*ctx* mutant infected mice (Extended Data Fig. 6e). As we observed with neonatal rabbits (Fig. 1d), the WT strain was recovered in significantly higher numbers in the luminal contents of the small intestine and cecum relative the Δ*ctx* mutant, while no difference was observed for tissue-associated bacteria or at an early time-point (6 hr post-infection) (Extended Data Fig. 6f and 6g). We next investigated whether heme uptake was important for CT-enhanced colonization through mutant analysis. *V. cholerae* encodes three receptors for heme uptake and the receptor, HutA, has previously shown to be required for utilization of hemoglobin as an iron source[19]. Interestingly, *hutA* (VCA0576) was the most highly expressed Fur-regulated gene in WT *V. cholerae* relative to the Δ*ctx* mutant in both the ileum and cecum (Supplementary Table 3). Furthermore, genetic ablation of either *hutA* or *viuA* (the later encoding the vibriobactin receptor) leads to a modest growth defect in the gut, which could be complemented by expression of these genes on a low-copy plasmid (Extended Data Fig. 7a). A *V. cholerae* double mutant of *hutA* and *viuA* has a reported pronounced growth defect in both neonatal mice and rabbits[19,20]. To investigate whether CT-induced disease is required for heme and vibriobactin uptake to confer a fitness advantage to *V. cholerae*, mice were infected with either a 1:1 mixture of the wild type and a *hutA viuA* mutant or with a 1:1 mixture of the Δ*ctx* mutant and a Δ*ctx hutA viuA* mutant. While the CT-producing *V. cholerae* exhibited a fitness advantage over the *hutA viuA* mutant in the gut, no fitness advantage was observed in mice inoculated with a 1:1 mixture of the Δ*ctx* mutant and a Δ*ctx hutA viuA* mutant (Fig. 2d). Additionally, oral administration of purified CT rescued the growth and the fitness advantage of the Δ*ctx* mutant over the Δ*ctx hutA viuA* mutant (Fig. 2d). Collectively, these data suggest that CT induces iron-depletion and luminal heme release *in vivo* (perhaps involving capillary congestion) and these host responses drive heme utilization and luminal growth of *V. cholerae*.

Iron is essential for bacterial metabolism. We found that metabolic pathways were the highest up-regulated genes in *V. cholerae* during colonization of the ileum relative to the cecum (Fig. 3a). Notably, genes involved in TCA cycle metabolism, L-Lactate utilization, and LCFA utilization were significantly up-regulated in the WT in the ileum relative to the Δ*ctx* mutant during infection (Fig. 3b-c and Extended Data Fig. 7b). Importantly, iron-sulfur cluster-containing TCA cycle enzymes encoding the succinate dehydrogenase (*sdh* operon), the iron-sulfur assembly protein cysteine desulfurase (VC0748), as well as other iron-binding proteins involved in metabolism, were highly expressed and up-regulated in the WT relative to the Δ*ctx* mutant during infection (Extended Data Fig. 7c, Supplementary Table 2). These data suggest that CT-induced disease enhances metabolism in *V. cholerae*, which in turn, might exacerbate iron depletion in the gut lumen through explosive bacterial growth and iron uptake.

The presence of LCFAs has previously been reported in the intestinal lumen of neonatal rabbits infected with *V. cholerae*[10]. Elevation of cAMP by CT activates eukaryotic Protein Kinase A, which in turn activates hormone-sensitive lipase, leading to lipolysis in target cells[21]. Hydrolysis of triacylglycerol stores results in liberation of glycerol and LCFAs[22]. Elevation of cAMP by CT can also induce a switch in host cell metabolism, leading to reduced oxygen consumption and increased lactic acid production[23]. Remarkably, WT infected rabbits had elevated concentrations of both LCFAs and L-Lactate in the lumen of the ileum relative to Δ*ctx* mutant infected animals (Fig. 3d and 3e) and elevated concentrations of LCFAs in the ileum in CT-treated mice (Extended Data Fig. 6h). Collectively, these data indicate that *V. cholerae* infection leads to a CT-dependent increase in LCFAs and L-Lactate in the small intestine lumen.

The uptake of exogenous LCFAs in bacteria requires the outer membrane transport protein, FadL[24]. The *V. cholerae* genome encodes three *fadL* homologs[12]. Our transcriptome analysis indicated that the *fadL* homolog, VC1043, was highly expressed in the ileum of infant rabbits and up-regulated in the WT relative to the Δ*ctx* mutant (Extended Data Fig. 7b and Supplementary Table 2). To investigate whether LCFA-uptake confers a fitness advantage to *V. cholerae* in the gut, we infected mice with a 1:1 mixture of WT and a *fadL* mutant (VC1043). The WT was recovered in significantly higher numbers from the small intestine (s.i) than the *fadL* mutant, suggesting that LCFA-uptake confers a fitness advantage to *V. cholerae* during infection (Fig. 3f). To determine whether CT-induced disease was required for LCFA-uptake mediated growth of *V. cholerae*, we infected mice with a 1:1 mixture of the Δ*ctx* mutant and Δ*ctx fadL* double mutant. In the absence of CT production, LCFA-uptake no longer conferred a fitness advantage to *V. cholerae* (Fig. 3f). Furthermore, oral administration of purified CT rescued the growth and the fitness advantage of the Δ*ctx* mutant over the Δ*ctx fadL* mutant (Fig. 3f). Interestingly, one WT *V. cholerae* sample collected from the rabbit ileum was found to have low expression of *ctxA* during infection and elevated concentrations of iron in the ileum relative to infected rabbits that had relatively high expression of *ctxA* (Extended Data Fig. 7d and 7e). The low expression of *ctxA* in this animal correlated with low expression of *hutA*, *viuB*, *fadL*, and *lldD* in the gut, similar to what was observed in a Δ*ctx* mutant infected animals.

We conclude that modulation of the host cell metabolism by CT produced by *V. cholerae in vivo* creates an iron-depleted intestinal niche that allows for enhanced growth of this organism through pathogen acquisition of host-derived nutrients including heme and LCFAs, and possibly L-lactate[25]. This conclusion may be relevant to the emergence and fitness of *V. cholerae* as a human pathogen in that genes induced by iron depletion *in vitro* are highly expressed in bacteria present in the stools of cholera patients[26]. Recent, highly successful variant strains of *V. cholerae* have also been reported to produce much more CT than earlier 7th pandemic strains[27]. Our results provide a new paradigm for how a microbial toxin enhances the growth of a pathogen and promotes its own transmission by remodeling both host and microbial metabolism.

METHODS

Bacterial strains

V. cholerae and *E. coli* strains used in this study are listed in Supplementary Table 4. Unless indicated otherwise, bacteria were routinely grown aerobically at 37°C in LB broth or on LB plates. Antibiotics were added to the media at the following concentrations: 0.1 mg/ml streptomycin, 0.02 mg/ml chloramphenicol (*E. coli*), 0.005 mg/ml chloramphenicol (*V. cholerae*), and 0.1 mg/ml carbenicillin.

In vitro iron depletion

For *in vitro* iron depletion and heme supplementation, overnight cultures of *V. cholerae* were grown in LB broth with DMSO (control), LB broth supplemented with 300 μM 2,2′-dipyridyl, or with LB broth supplemented 300 μM 2,2′-dipyridyl and 5uM hemin and cells were harvested when the bacterial growth reached approximately an OD600 of 0.9.

Construction of plasmids

The plasmids and primers used in this study are listed in Supplementary Table 5 and 6, respectively. PCR products were cloned into vectors using Gibson Assembly (New England Biolabs, Ipswich, MA) and sequenced.

A suicide plasmid for generating a deletion of *ctxA* and *ctxB* was constructed by using primers del_A and del_B to PCR amplify a 557 bp 5′ flanking sequence that included 9 nucleotides of the *ctxA* coding region. Primers del_C and del_D were used to PCR amplify a 515 bp fragment that included 3 nucleotides of the 3′ coding region of *ctxB*. The two PCR fragments resulting in-frame *ctxAB* operon deletion were cloned into pDS132 using Gibson Assembly to generate plasmid pFRC1.

An internal fragment of the *fadL* gene was amplified by PCR using the primers listed in Supplementary Table 6. The *fadL* PCR product was then cloned into pGP704 using Gibson Assembly to create pFRC5. A fragment of the *hutA* gene was amplified by PCR and cloned into pGP704 using Gibson Assembly to create pFRC9. A fragment of the *viuA* gene was amplified by PCR and cloned into pEP185.2 using Gibson Assembly to create pFRC10.

For complementation of the *hutA*, *viuA*, and *fadL* mutants, the open reading frame including the promoter region was amplified using the primers listed in Supplementary Table 6. The

resulting PCR fragment was cloned into pWSK29 using Gibson Assembly to create pFR11, pFR12, and pFR13, respectively.

Construction of *V. cholerae* mutants

Suicide plasmids were propagated in *E. coli* DH5α λ*pir* and introduced into the *V. cholerae* strain El Tor strain C6706 by conjugation using *E. coli* S17-1 λ*pir* as a donor strain.

The *ctxAB* operon was deleted by introduction of pFRC1 into *V. cholerae* C6706. Transconjugants were selected for on LB plates containing Strep and Cm. Sucrose counter-selection was performed as described previously[28]. A strain that was sucrose-tolerant and Cm^s was verified by PCR to carry a deletion in the *ctxAB* operon and was denoted FRC38.

Exconjugants were selected on LB agar plates containing streptomycin and antibiotics selecting for integration of the suicide plasmid. Integration of the plasmids in the correct location on the chromosome was verified by PCR. Using this methodology, pFRC5, pFRC9, and pFRC10 were integrated into the *fadL, hutA*, and *viuA* genes of C6706 to yield strains FRC122, FRC127 and FRC128, respectively.

pFRC5 and pFRC10 were integrated into the *fadL* and *viuA* genes of FRC38 to yield strains FRC123 and FRC130, respectively.

pFRC9 was integrated into the *hutA* gene of strain FRC130 to yield FRC131.

Animal Experiments

All animal experiments in this study were approved by the Institutional Animal Care and Use Committee at Harvard Medical School.

Rabbit Experiments.—Infant rabbits were infected with *V. cholerae* as previously described[9] with the following modifications. Three-day-old infant rabbits ($N = 4$) were treated with Zantac (2 mg/kg body weight) intraperitoneally and 3 hours later orally inoculated with 0.5 ml of 2.5% sodium bicarbonate (mock infection) or with 1×10^9 colony forming units (CFU) of *V. cholerae* wild type or the Δ*ctxAB* mutant in 0.5 ml of 2.5% sodium bicarbonate. One-day post-infection, rabbits were euthanized and samples from the gastrointestinal tract were collected for RNA purification and bacteriological analysis. Independent infant rabbit litters were used for infection with each strain. Rabbits from different litters are indicated under the “Litter” number in the source data files. Fig. 1, Fig. 2a-c, Fig. 3a-e, Extended Data Fig. 2, Extended Data Fig. 3, Extended Data Fig. 4, and Extended Data Fig. 5, Extended Data Fig. 7b-e, represent data from four independent rabbit litters (litter 1: wild type infected, litter 2: Δ*ctxAB* mutant infected #1, litter 3: mock infected, litter 4: Δ*ctxAB* mutant infected #2). Animals were randomly allocated in treatment groups. Group sizes (at least four animals per treatment group) represents the minimum number animals needed to reach statistical significance ($p < 0.05$) between experimental groups. The Δ*ctxAB* mutant infection group was repeated in an independent litter of infant rabbits. Animals that were euthanized before an experimental endpoint due to health concerns were excluded from the analysis.

Mouse Experiments.—Suckling mice were infected with *V. cholerae* as previously described[29] with the following modifications. CD-1 mice were obtained from Charles River Laboratories (Wilmington, MA, USA). 4-day old CD-1 suckling mice separated from their mothers were randomly allocated in treatment groups and 2 hours later orally inoculated with 0.05 ml sterile LB broth (mock infection) or with 1×10^7 CFU of *V. cholerae* in 0.05 ml LB broth. For competitive infections, mice were infected with an equal mixture of 5×10^6 CFU of each *V. cholerae* strain in 0.05 ml LB broth. To determine the competitive index (CI), the ratio of recovered wild-type bacteria to mutant bacteria (output ratio) was divided by the ratio present in the inoculum (input ratio). Mice from different litters are indicated under the "Litter" number in the source data files. In Fig. 2d, a litter of mice (litter 1) were randomly allocated in treatment groups and infected with either the wild type vs. *viuA hutA* or Δ*ctxAB* vs. Δ*ctxAB viuA hutA*. The wild type vs. *viuA hutA* experiment was repeated in an independent litter (litter 3). In Fig. 3f, a litter of mice (litter 1) were randomly allocated in treatment groups and infected with either the wild type vs. *fadL* or Δ*ctxAB* vs. Δ*ctxAB fadL*. The wild type vs. *fadL* experiment was repeated in an independent litter (litter 3). In Extended Data Fig. 1 and Extended Data Fig. 6f (Δ*ctxAB* + CT CFU data), mice from one litter (litter 6) were randomly allocated in treatment groups and infected with either the wild type vs. Δ*ctxAB* or with Δ*ctxAB* + 10 μl CT. In Extended Data Fig. 6b, mice from one litter (litter 1) were randomly allocated in treatment groups and infected with either the wild type or Δ*ctxAB* mutant and a second litter of mice (litter 2) was mock treated for qRT-PCR analysis. In Extended Data Fig. 6c, two independent litters (litter 3 and litter 4) were randomly allocated in treatment groups and infected with either the wild type or Δ*ctxAB* mutant. Mice from an independent litter (litter 5) were randomly allocated in treatment groups and mock treated or treated with with 10 μl CT. For the 6 hrs p.i data, mice from one litter (litter 8) were randomly allocated in treatment groups and infected with either the wild type or Δ*ctxAB* mutant. In Extended Data Fig. 6d, mice from one litter (litter 9) were randomly allocated in treatment groups and infected with either the wild type or Δ*ctxAB* mutant. Hemin data for mock or 10 μl CT treated mice was generated from same experiment (litter 5) as shown in Extended Data Fig. 6c. For Extended Data Fig. 6e, mice from one litter (litter 10) were randomly allocated in treatment groups and infected with either the wild type or Δ*ctxAB* mutant. In Extended Data Fig. 6f, CFU data shown was generated from litters shown in Extended Data Fig. 6c (matching litter numbers). Mice from an independent litter (litter 11) were randomly allocated in treatment groups and infected with either the wild type or Δ*ctxAB* mutant to reproduce data in Data Fig. 6f. In Extended Data Fig. 6g, 6 hrs p.i CFU data was generated from same experiment (litter 8) as shown in Extended Data Fig. 6c. In Extended Data Fig. 6h, LCFA data was generated from same experiments (litter 5 and litter 9) as shown in Extended Data Fig. 6d. In Extended Data Fig. 7a, mice from one litter (litter 1) were randomly allocated in treatment groups and infected with either wild type vs. *hutA* or wild type vs. *viuA*. Mice from a second litter (litter 2) were randomly allocated in treatment groups and infected with either pWSK29::*hutA* vs. *hutA*(pWSK129) or pWSK29::*viuA* vs. *viuA*(pWSK129). Mice from a third litter (litter 3) were infected with pWSK29::*fadL* vs. *fadL*(pWSK129). In Extended Data Fig. 1b, Extended Data Fig. 6d, Extended Data Fig. 6e, Extended Data Fig. 6f (CFU/g tissue), and Extended Data Fig. 6g, neonates from one litter were randomly assigned for infection with the wild type or the Δ*ctxAB* mutant and the individual neonate is the experimental unit "N" for statistical

analysis (within-litter design). For treatment with purified cholera toxin (CT), mice were treated by oral gavage with 10 μg of purified CT (List Biological Laboratories, Campbell, CA) in 0.05 ml LB broth or by mixing 10 μg of purified CT with 0.05 ml containing the indicated *V. cholerae* inoculum. After euthanasia, gastrointestinal tracts were collected approximately 22 hours post-infection for histopathological and bacteriological analysis. The ileum was defined as the last 4 cm of the distal small intestine. The fluid accumulation ratio (FA) ratio in mice was determined by weight of entire gastrointestinal tract (gut) / (mouse body weight - gut weight), as previously described[30]. Group sizes (at least four animals per treatment group) represents the minimum number animals needed to reach statistical significance ($p < 0.05$) between experimental groups. Animals that were euthanized before an experimental endpoint due to health concerns were excluded from the analysis. Mouse samples were blinded for histopathology analysis.

Histopathology

Formalin fixed small intestine tissue sections were stained with hematoxylin and eosin at the Harvard Medical School Rodent Histopathology Core. Capillary congestion was confirmed by a veterinary pathologist. Representative images were obtained using a Nikon TE2000 inverted microscope and the brightness adjusted (Adobe Photoshop CS2).

RNA isolation of *in vivo* samples

Luminal samples from the ileum and cecum of 3-day old infant rabbits infected with *V. cholerae* were snap-frozen in liquid nitrogen for subsequent phenol:chloroform RNA isolation. Contaminating DNA was removed using the DNA-free kit (Applied Biosystems) and RNA was stored at −80°C.

In vivo transcriptome analysis using Illumina RNA sequencing

The Ovation Complete Prokaryotic RNA-Seq Library Systems (NuGEN) was used for cDNA synthesis and library preparation of 200 bp (mean size) fragments. cDNA library quantification was performed using the Agilent 2200 TapeStation. RNA-sequencing library quantification was performed on HiSeq 2500 Rapid PE V2 by 100 bp paired-end high-throughput sequencing. The raw reads in FASTQ format were aligned to chromosomes I and II of the *V. cholerae* El Tor N16961 genome (RefSeq accession numbers NC_002505 and NC_002506) using the bowtie2[31] algorithm on Geneious 10.0 (http://www.geneious.com)[32]. Differential expression and PCA analysis was performed on Geneious using DEseq 2[33]. Venn diagram was made using Venny 2.1 (Oliveros, J.C. (2007-2015) Venny. An interactive tool for comparing lists with Venn's diagrams. http://bioinfogp.cnb.csic.es/tools/venny/index.html). Bioinformatics for metabolic pathway analysis was performed using DAVID[34]. Upregulated genes were defined as having a positive log2 fold change and adjusted p-value of less than 0.0001.

Quantitative real-time PCR

Reverse transcription (RT) and Quantitative real-time PCR (qRT-PCR) was performed using 50ng of DNase treated RNA with the KAPA SYBR FAST One-Step (Kapa biosystems) kit.

The fold-change of gene expression was calculated by using the comparative CT method[35] with the housekeeping genes *gyrB* for *V. cholerae* and GAPDH for mice.

RNA-seq heatmap

RNA-seq heat map of *V. cholerae fur*-regulated genes was created using Cluster 3.0 (http://bonsai.hgc.jp/~mdehoon/software/cluster/software.htm) and Java TreeView (http://jtreeview.sourceforge.net) software packages from mean-centered log2 transformed expression values (RPKM).

Iron measurements by ICP-MS

Luminal samples from the ileum of infant rabbits were snap-frozen in liquid nitrogen. Samples were first treated with concentrated nitric acid (65%-70%) for 24 hours to kill bacteria. Sample analysis was performed by Brooks Applied Labs (Bothell, WA). Briefly, samples were digested in their entirety with a mix of concentrated nitric acid and hydrochloric acid by the EPA Method 3050B and iron was measured by triple quadrupole ICP-MS using the Agilent 8800.

Heme measurements

Samples from fluid of the ileum and cecum of infant rabbits were centrifuged and the supernatant was sterilized using a 0.2 μm filter. Heme levels from filtered samples were measured using the hemin assay kit (ab65332, Abcam, Cambridge, UK) according to the manufacturer's instructions.

LCFA measurements

Samples from fluid of the ileum and cecum of infant rabbits were centrifuged and the supernatant was sterilized using a 0.2 μm filter. LCFAs (C-8 octanoate and longer) from filtered samples were measured using the Free Fatty Acid Assay Kit (ab65341) according to the manufacturer's instructions.

L-Lactate measurements

Samples from fluid of the ileum and cecum of infant rabbits were centrifuged and the supernatant was sterilized using a 0.2 μm filter. L-Lactate levels from filtered samples were measured using the L-Lactate assay kit (ab65331, Abcam, Cambridge, UK) according to the manufacturer's instructions.

Lipocalin-2 ELISA

Samples from fluid of the ileum and cecum of infant rabbits were centrifuged and the supernatant was sterilized using a 0.2 μm filter. Lipocalin-2 levels from filtered samples were measured using the Rabbit Lipocalin-2 (LCN2) ELISA Kit (MBS017878, MyBioSource, San Diego, CA, USA) according to the manufacturer's instructions.

Statistical analysis

RNA-seq differential expression analysis p-values were determined and adjusted for multiple testing by the Benjamini-Hochberg method using the R package DESeq2.

Statistical analyses were performed with Prism software (GraphPad). Fold changes of ratios were transformed logarithmically prior to statistical analysis. An unpaired two-tailed Student's *t*-test was used to determine whether differences in fold-changes between two groups were statistically significant ($P < 0.05$). For comparisons between three or more groups, one-way ANOVA (between-subjects factors) or two-way ANOVA (between-subjects factors) was used followed by post hoc multiple comparisons test. F-statistics (F(Dfn, DFd)) are shown in the figure legends for one-way ANOVA and in Supplementary Table 7 for two-way ANOVA. Outliers were determined with Prism using the ROUT method ($Q = 0.5$) from log transformed fold-change expression values. Outlier for *ctxA* expression was excluded from statistical analysis.

Data availability

The data that support the findings of this study are available from the corresponding author upon request. The RNA-Seq data have been deposited in the Gene Expression Omnibus (https://www.ncbi.nlm.nih.gov/geo) under the accession number: GSE132653.

Extended Data

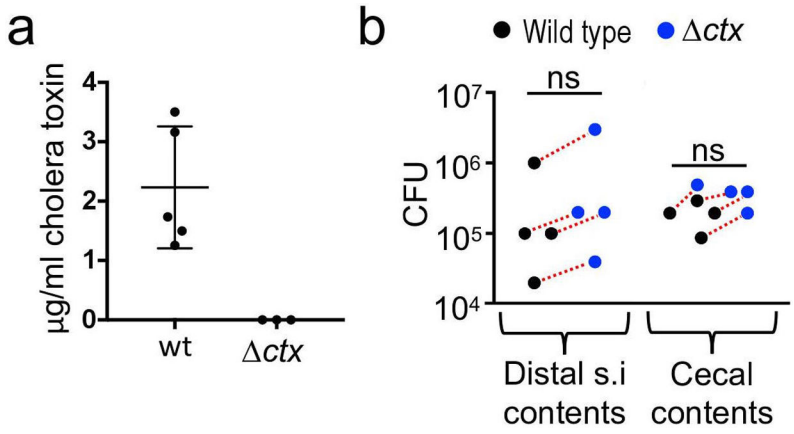

Extended Data Figure 1. *V. cholerae* CT production rescues Δ*ctx* mutant growth (related to Figure 1).

(a) GM-1 cholera toxin ELISA assay from filtered supernatant of *V. cholerae* C6706 wild type (wt) ($N = 5$) or cholera toxin mutant (Δ*ctx*) ($N = 3$) grown *in vitro* under cholera toxin-inducing (AKI) conditions. Error bars represent means ± SD. (b) Groups of CD-1 mice ($N = 4$) were infected with a 1:1 mixture of the *V. cholerae* WT and the Δ*ctx* mutant. The competitive index (CI; the ratio of strains recovered) was determined one day after infection. Dotted red lines connect strains recovered from the same animal. Bacterial numbers were compared by unpaired two-sided student *t*-test. Each dot represents data from an individual animal or experiment. ns, not statistically significantly different.

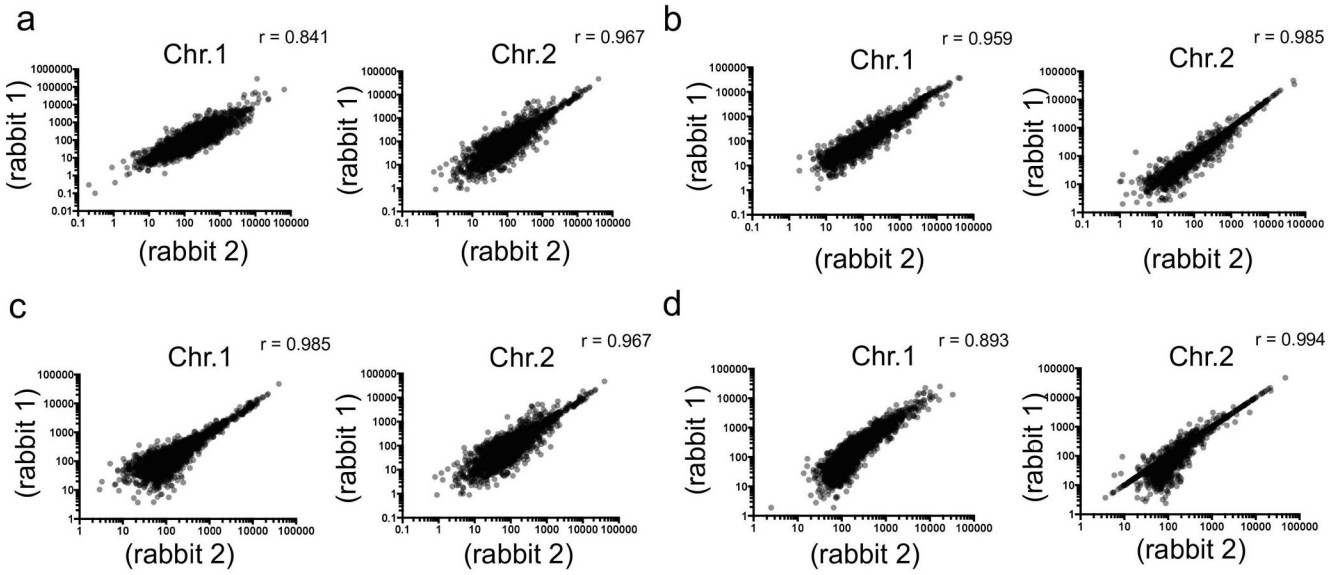

Extended Data Figure 2. RNA-seq analysis of *V. cholerae in vivo* gene expression (related to Figures 1-3).

(a-d) RNA-seq normalized expression (RPKM = reads mapping to gene)/(length of gene/1000)/(total reads mapped to *V. cholerae* genome/1000000) from wild type or Δ*ctx* mutant *V. cholerae* during infection of 3-day old infant rabbits. Total expression from chromosome I (Chr. I) or chromosome II (Chr. II) from wild type infecting the ileum (a) or cecum (b) or the Δ*ctx* mutant infecting the ileum (c) or cecum (d). Correlations (r) are shown between biological replicates (rabbit 1 and rabbit 2).

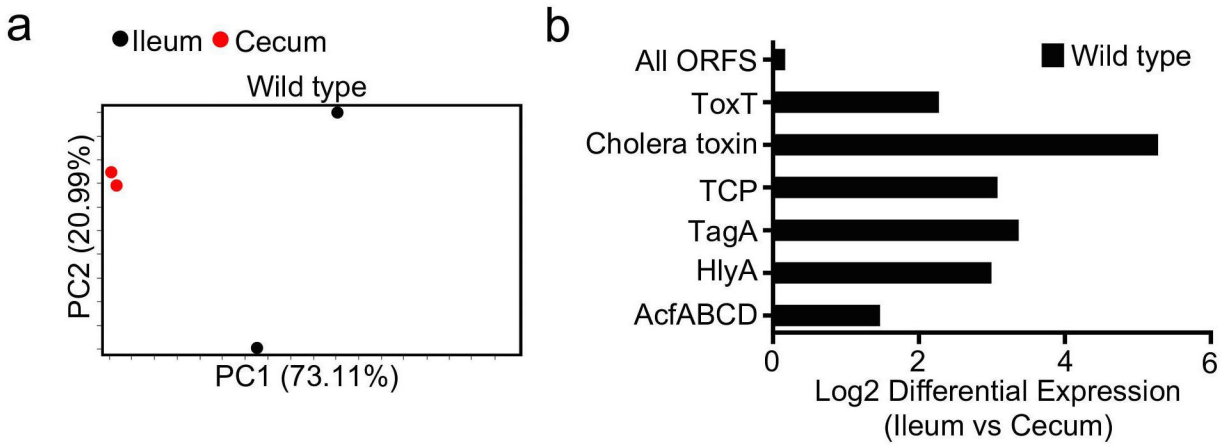

Extended Data Figure 3. RNA-seq analysis of the wild type C6706 during colonization of the ileum and cecum (related to Figure 1).

(a-b) RNA-seq analysis of *Vibrio cholerae* in the ileum and cecum during infection of infant rabbits. (a) PCA plots for RNA-seq data from two biological replicates of *V. cholerae* wild type from the ileum (black circles) or cecum (red circles) of infant rabbits ($N = 2$). (b) Differential expression of all *V. cholerae* ORFs and genes involved in virulence. ToxT (VC0838), Cholera Toxin (VC1456-VC1457), Toxin-Coregulated Pilus (TCP) (VC0825-VC0837), TagA (VC0820), HlyA (VCA0219), and Accessory Colonization Factors (Acf) (VC0840-0844) in the wild type during colonization of the ileum relative to the cecum.

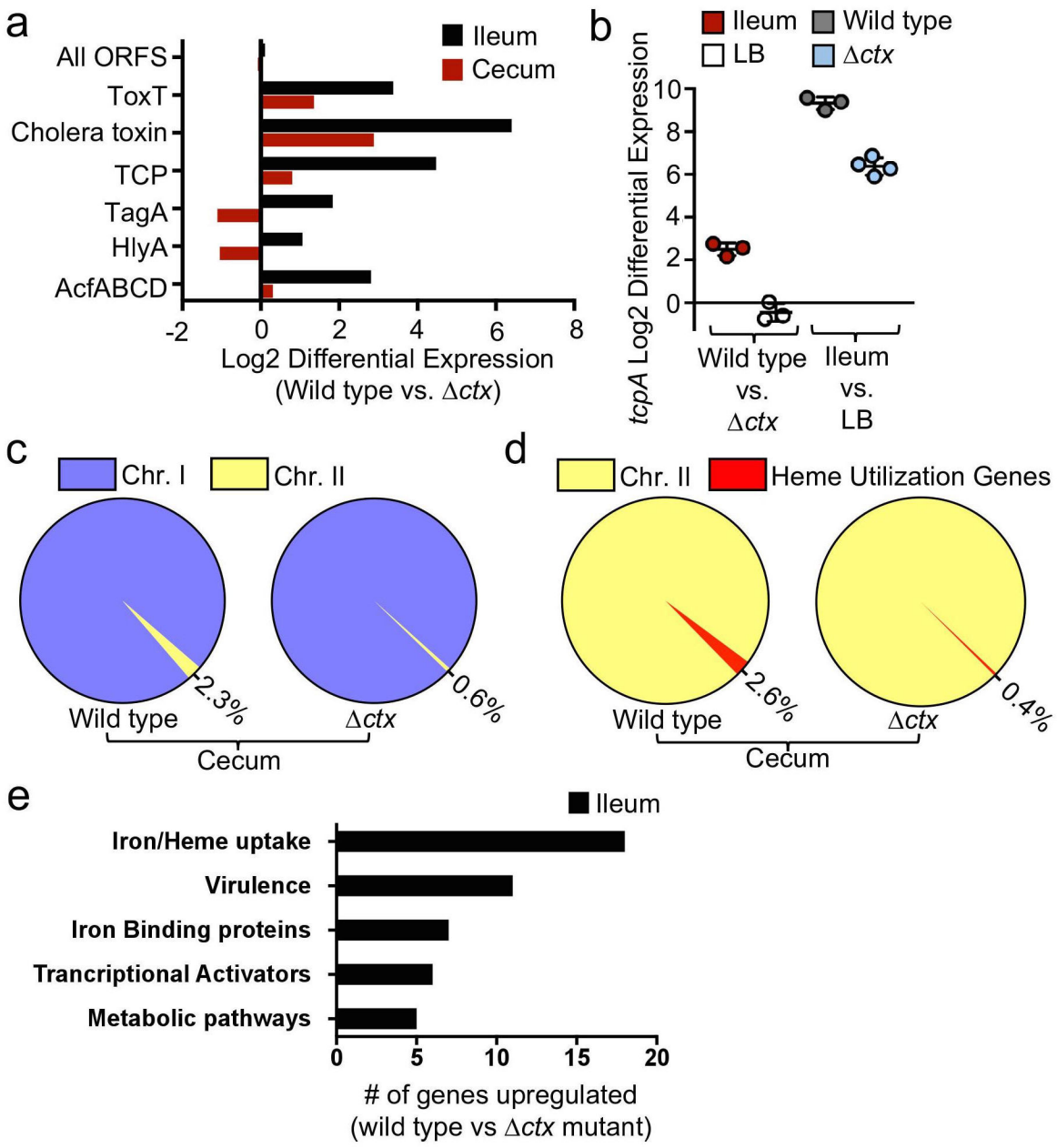

Extended Data Figure 4. RNA-seq analysis of CT-dependent *V. cholerae* gene expression during colonization of the gut (related to Figures 1-2).

(a-e) RNA-seq analysis of *Vibrio cholerae* in the ileum and cecum during infection of infant rabbits. (a) Differential expression of all *V. cholerae* ORFs and genes involved in virulence. ToxT (VC0838), Cholera Toxin (VC1456-VC1457), Toxin-Coregulated Pilus (TCP) (VC0825-VC0837), TagA (VC0820), HlyA (VCA0219), and Accessory Colonization Factors (VC0840-0844) in the wild type relative to the cholera toxin mutant (Δ*ctx*) during infection of the ileum or cecum. (b) Transcript levels of *tcpA* were determined by quantitative real-time PCR in the wild type ($N = 3$) relative to the cholera toxin mutant (Δ*ctx*) ($N = 4$) colonizing the ileum (red circles), in LB (white circles) ($N = 3$) and in the ileum relative to LB in the wild type (grey circles) and cholera toxin mutant (Δ*ctx*) (light

blue circles). Error bars represent means ± SD. (c) Percent abundance of raw RNA-seq reads aligned to chromosome I (Chr. I; purple) or chromosome II (Chr. II; yellow) from wild type or the cholera toxin mutant (Δ*ctx*) in the cecum. (d) Percent abundance of heme utilization genes (VCA0907-VCA0915, VCA0576; red) from raw RNA-seq reads aligned to chromosome II (Chr. II; yellow) from wild type or the cholera toxin mutant (Δ*ctx*) in the cecum. (e) DAVID bioinformatics pathway analysis from RNA-seq data of significantly upregulated pathways (positive log2 fold change and adjusted p-value of less than 0.0001) in the wild type relative to the cholera toxin mutant (Δ*ctx*) during colonization of the ileum of infant rabbits ($N = 2$). RNA-seq differential expression analysis p-values were determined and adjusted for multiple testing by the Benjamini-Hochberg method using the R package DESeq2.

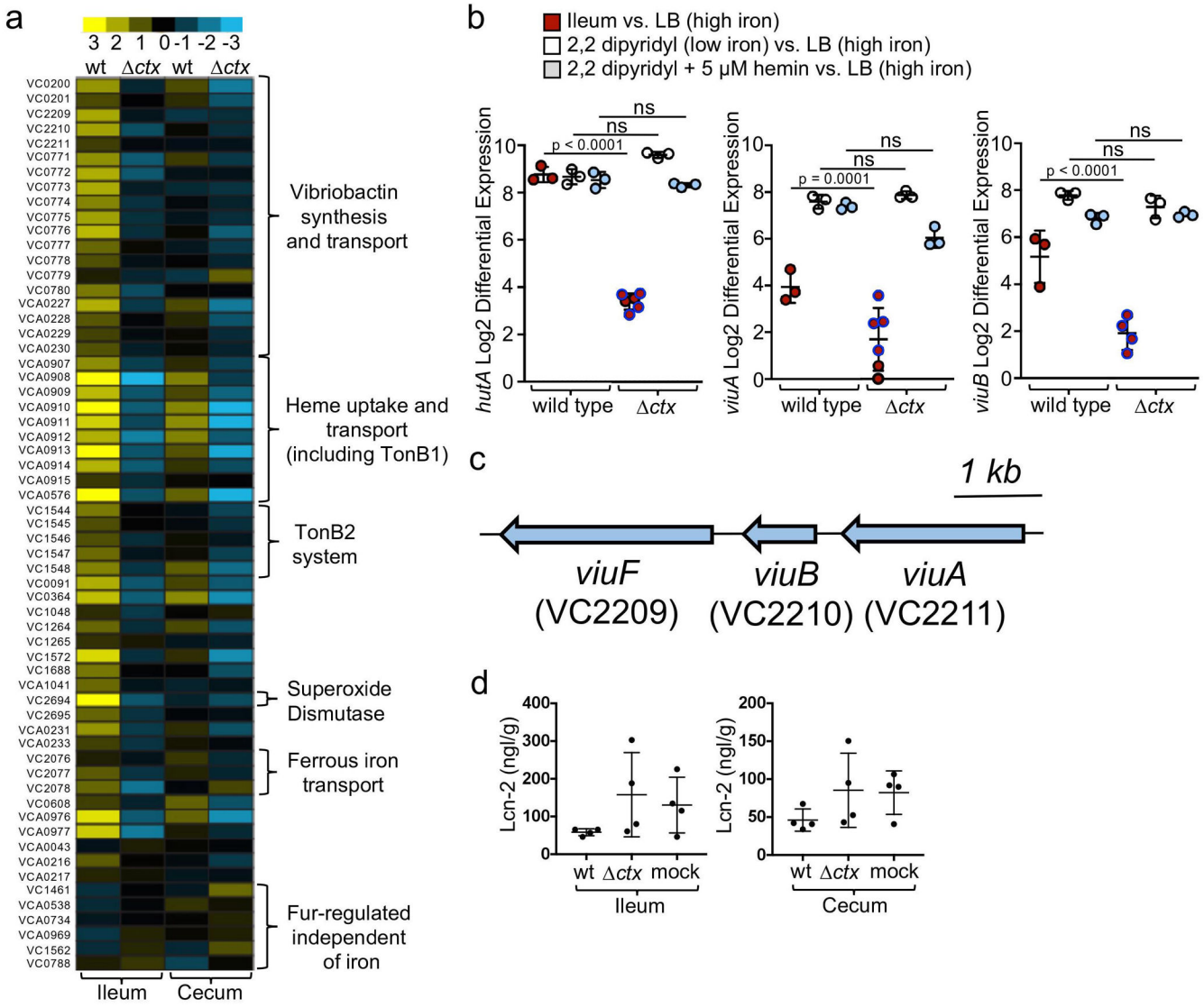

Extended Data Figure 5. RNA-seq analysis of the *Vibrio cholerae fur* regulon during infection of infant rabbits (related to Figures 1-2).

(a) Heat-map of RNA-seq data from normalized expression (RPKM) of *Vibrio cholerae fur* regulated genes (listed in Supplementary Table 3) in the wild type relative and the cholera toxin mutant (Δ*ctx*) during colonization of the ileum or cecum of infant rabbits. (b) Differential expression of *hutA*, *viuA*, and *viuB* was determined by quantitative real-time PCR analysis from *V. cholerae* wild type or the cholera toxin mutant (Δctx) in the ileum (*N* = 3 wild type *hutA*, *viuA*, and *viuB*; *N* = 6 for Δctx *hutA* and *viuA*, *N* = 4 for Δctx *viuB)* or in *V. cholerae* wild type or the cholera toxin mutant (Δctx) grown in LB (*N* = 3), in LB with 2,2 dipyridyl (*N* = 3), or in LB with 2,2 dipyridyl and hemin (*N* = 3). Error bars represent means of log2 transformed mRNA levels determined by quantitative real-time PCR from ileum relative to LB (red circles), LB with 2,2 dipyridyl relative to LB (white circles), and LB with 2,2 dipyridyl and hemin relative to LB (grey circles) ± SD. A two-way ANOVA (Supplementary Table 7) was used to compare normalized expression (ddCT) values between the strains (wt and Δctx mutant) for each treatment (Ileum, 2,2 dipyridyl, 2,2

dipyridyl + 5 μM hemin, and LB) followed by a post-hoc Sidak's multiple comparisons test. Blue lines on red circles distinguish animals from different litters of Δ*ctx* infected infant rabbits. (c) Schematic representation of the genetic region for *viuA*, *viuB*, and *viuF*. ns, not statistically significantly different. (d) Luminal Lipocalin-2 levels determined by ELISA from the ileum and cecum of infant rabbits ($N = 4$) that were mock-infected or infected with the wild type (wt) or the cholera toxin mutant (Δ*ctx*). Error bars represent means ± SD.

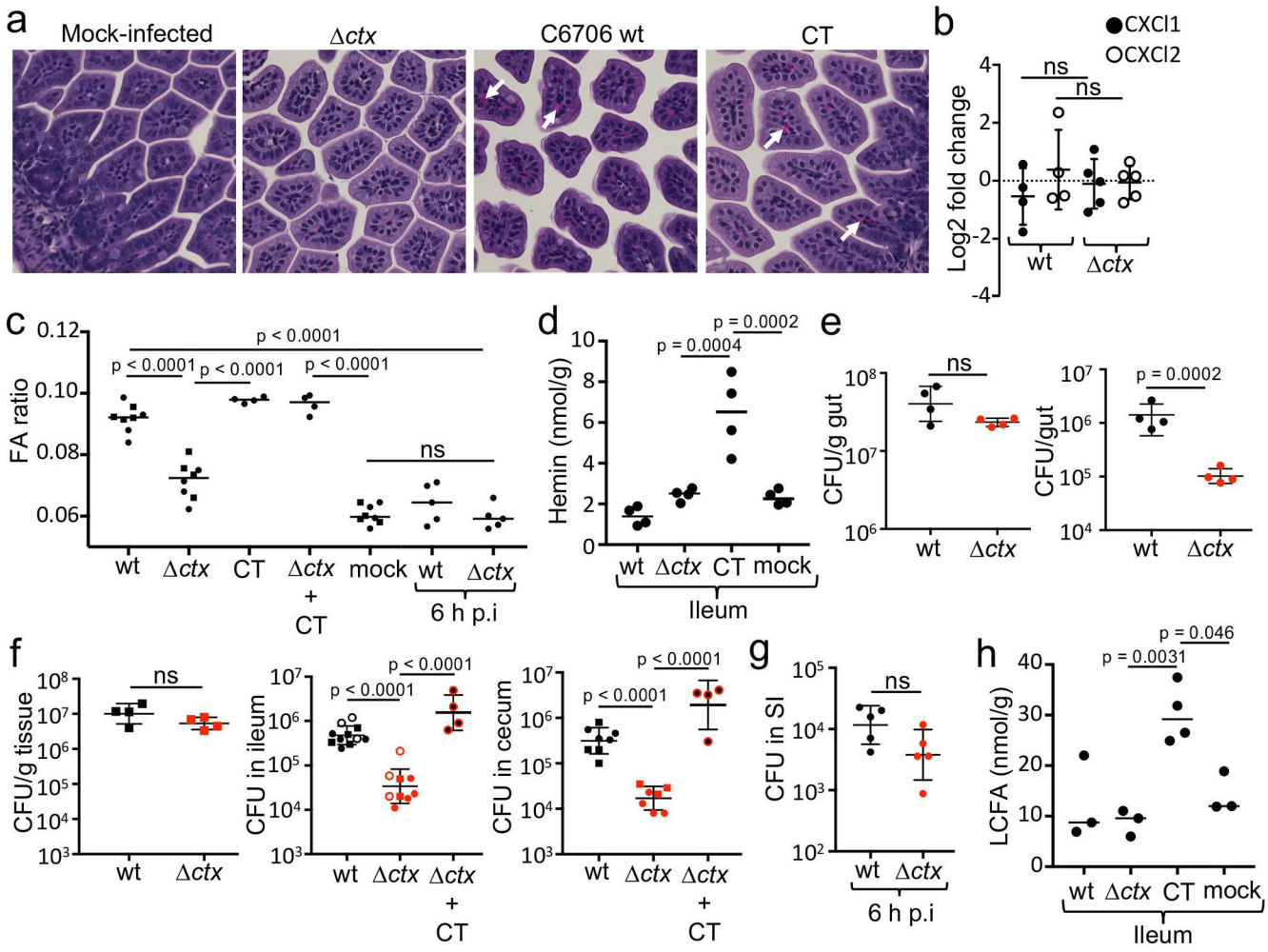

Extended Data Figure 6. Cholera toxin induces capillary congestion and enhances luminal growth of *V. cholerae* in a mouse model of infection (related to Figures 1-3).

(a-h) Groups of CD-1 mice were mock-infected or infected intragastrically with the wild type (wt), the cholera toxin mutant (Δ*ctx*), the Δ*ctx* mutant mixed with purified CT, or treated orally with purified cholera toxin (CT) and samples were collected one day after infection. (a) Representative images of H/E-stained ileum tissue sections showing capillary congestion (arrows) from mice infected with the indicated strains or treated orally with purified CT. All images were taken at 60X magnification. (b) Expression of CXCl1 and CXCl2 in the ileal mucosa of mice ($N = 4$) was determined by quantitative real-time PCR analysis. Error bars represent means of CXCl1 and CXCl2 mRNA levels as fold-change over mRNA levels in mock-infected mice ± SD. An unpaired two-sided Student's *t*-test was used to compare the differences in fold-changes between the wt and Δ*ctx* mutant. (c) The fluid accumulation ratio (FA) ratio for mice ($N = 8$ for wild type, Δ*ctx*, and mock; $N = 4$ for CT, and Δ*ctx* + CT, $N = 5$ for wild type, and Δ*ctx* 6 h.p.i) treated with the indicated strains or treated orally with purified CT. The FA ratios between the groups were compared using one-way ANOVA ($F(6, 35) = 66.03$, $p < 0.0001$) followed by post-hoc Tukey's multiple comparisons test. Black lines show median for individual animals (black circles). Different shapes indicate animals from different litters. (d) Luminal hemin measurements from the

ileum of mice ($N = 4$) treated with the indicated strains or treated orally with purified CT. Hemin levels in the CT-treated group were compared to the Δ*ctx* mutant and mock treated using one-way ANOVA ($F(3, 12) = 25.59$, $p < 0.0001$) followed by post-hoc Sidak's multiple comparisons test. Black lines show median for individual animals (black shapes). (e) The CFU/g and total CFU from the whole gastrointestinal tract (gut) from mice ($N = 4$) infected with wt or the Δ*ctx* mutant. An unpaired two-sided Student's *t*-test was used to compare the bacterial concentrations from wt and Δ*ctx* mutant infected animals. Error bars represent means ± SD. (f) The CFU/g tissue (ileum) ($N = 4$) and total CFU from the lumen of the ileum ($N = 11$ for wild type, $N = 9$ for Δ*ctx*, and $N = 4$ for Δ*ctx* + CT) or lumen of the cecum ($N = 8$ for wild type, $N = 7$ for Δ*ctx*, and $N = 4$ for Δ*ctx* + CT) of mice infected with the indicated *V. cholerae* strains. Different shapes indicate animals from different litters. An unpaired two-sided Student's *t*-test was used to compare the CFU/g tissue in wt and Δ*ctx* mutant infected animals. The wt CFU in the ileum or cecum were compared to the Δ*ctx* mutant or mock groups using one-way ANOVA (Ileum: $F(2, 21) = 50.24$, $p < 0.0001$; Cecum: $F(2, 16) = 51.6$, $p < 0.0001$) followed by post-hoc Sidak's multiple comparisons test. Error bars represent means ± SD. (g) The CFU in the lumen of the ileum 6 hours post-infection mice infected with *V. cholerae*. An unpaired two-sided Student's *t*-test was used to compare the CFU from wt and Δ*ctx* mutant infected animals. Error bars represent means ± SD (h) Luminal LCFA measurements (8 carbon chain or greater) from the ileum of mice ($N = 3$ for wild type, Δ*ctx*, and mock; $N = 4$ for CT) treated with the indicated strains or treated orally with purified CT. LCFA concentrations in the CT-treated group were compared to the Δ*ctx* mutant and mock groups treated using one-way ANOVA ($F(3, 9) = 7.814$, $P = 0.0071$) followed by post-hoc Sidak's multiple comparisons test. Black lines show median for individual animals (black circles). ns, not statistically significantly different.

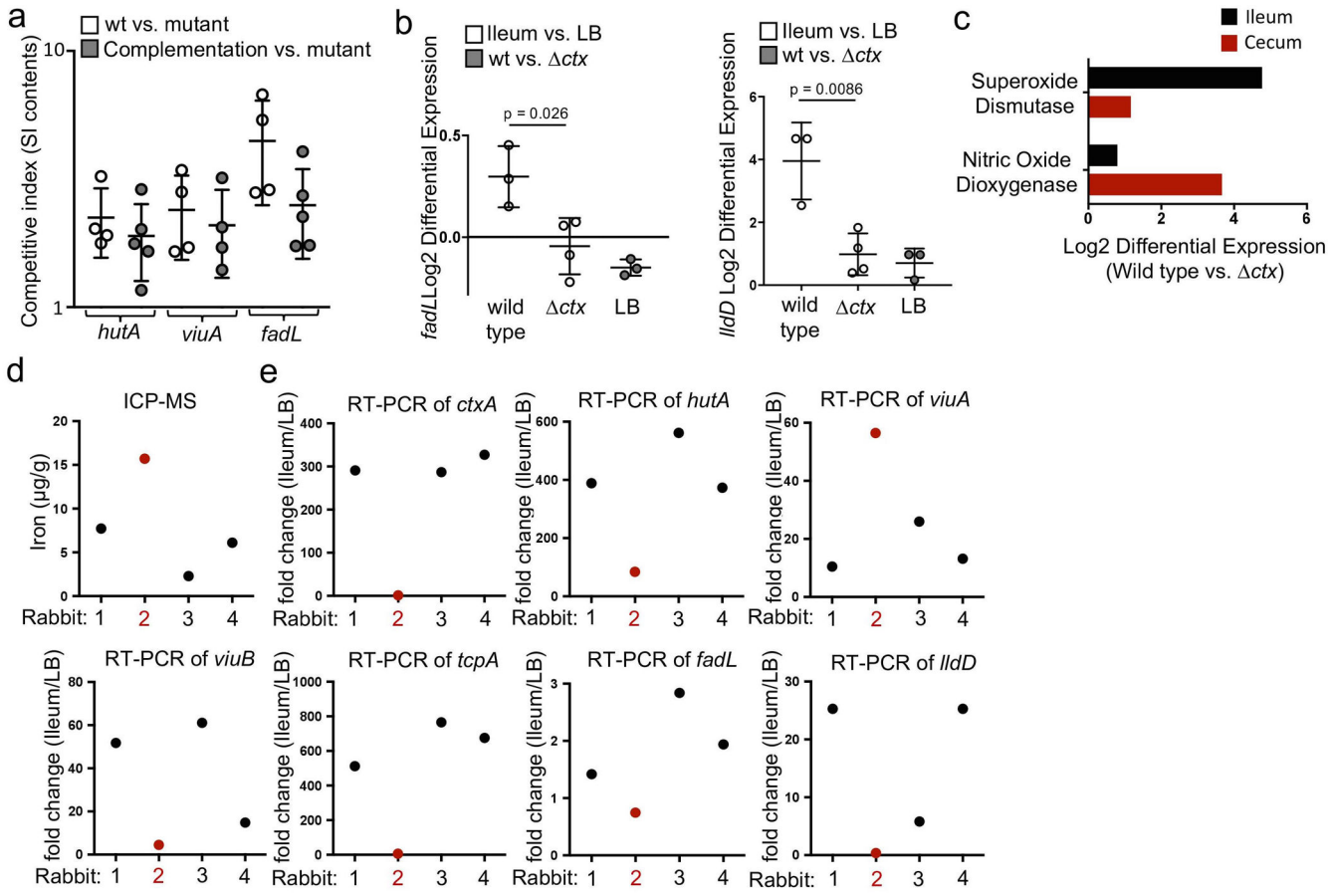

Extended Data Figure 7. Differential expression of CT-dependent metabolism-related genes in *V. cholerae* (related to Figures 1-3).

(a) Groups of CD-1 mice ($N = 4$) were infected with a 1:1 mixture of the wild type and the indicated mutant (white bars) or with a 1:1 mixture of the mutant harboring a control vector (pWSK129) and the mutant harboring the complemented gene in pWSK29 (grey bars). The competitive index for the wild type versus the *fadL* mutant from the first experiment ($N = 4$) in Fig. 3f is shown for comparison. The competitive index (CI; the ratio of strains recovered) was determined one day after infection. Error bars represent means ± SD. (b) Transcript levels of *fadL and lldD* were determined by quantitative real-time PCR in the wild type ($N = 3$) and cholera toxin mutant (Δ*ctx*) ($N = 4$) during colonization of the ileum relative to LB (white bars) and in the wild type relative to the cholera toxin mutant (Δ*ctx*) in LB (grey bars) ($N = 3$). An unpaired two-sided Student's *t*-test was used to compare the log2 fold-change in expression of *fadL* and *lldD* (ileum relative to LB) between wt and Δ*ctx* mutant. Error bars represent means ± SD. (c) Differential expression of *V. cholerae* Superoxide Dismutase (VC2694), and Nitric Oxide Dioxygenase (VCA0183) in the wild type relative to the cholera toxin mutant (Δ*ctx*) during colonization of the ileum or cecum. (d) Iron concentrations from the ileum of individual rabbits infected with the wild type *V. cholerae* for experiments shown in Figure 2b. (e) Fold-change of transcript levels of wild type *V. cholerae* genes: *ctxA* (VC1456), *hutA* (VCA0576), *viuA* (VC2211), *viuB* (VC2210), *tcpA* (VC0825), *fadL* (VC1043), and *lldD* (VCA0983) in the ileum relative to LB were determined by quantitative real-time PCR from individual rabbits in Extended Data Fig. 4b, 5b, and 7b. Dark red (rabbit

2) circle indicates data for sample collected with low expression of cholera toxin (*ctxA*) that was determined to be a statistical outlier using the ROUT method (Q = 0.5) from log transformed fold-change expression values.

Supplementary Material

Refer to Web version on PubMed Central for supplementary material.

Acknowledgements.

The authors thank Florencia Caro for advice on library preparation and RNA-seq analysis. We thank Yang Fu and Wenjing Zhao for technical advice on animal experiments and all other members of the Mekalanos laboratory for their helpful advice. We thank the staff at the Biopolymers Facility at HMS for Illumina sequencing, the staff of Brooks Applied Labs for ICP-QQQ-MS, and the Rodent Histopathology Core at HMS for tissue staining and histopathological analysis. This work was supported by grants AI-018045 and T32 AI007061 from the National Institute of Allergy and Infectious Disease and National Institute of Health (U.S.A.).

REFERENCES

1. Faruque SM, Albert MJ & Mekalanos JJ Epidemiology, genetics, and ecology of toxigenic Vibrio cholerae. Microbiol Mol Biol Rev 62, 1301–1314 (1998). [PubMed: 9841673]
2. Cassat JE & Skaar EP Iron in infection and immunity. Cell Host Microbe 13, 509–519, doi:10.1016/j.chom.2013.04.010 (2013). [PubMed: 23684303]
3. Henderson DP & Payne SM Cloning and characterization of the Vibrio cholerae genes encoding the utilization of iron from haemin and haemoglobin. Mol Microbiol 7, 461–469 (1993). [PubMed: 8384684]
4. De SN Enterotoxicity of bacteria-free culture-filtrate of Vibrio cholerae. Nature 183, 1533–1534 (1959). [PubMed: 13666809]
5. Cassel D & Pfeuffer T Mechanism of cholera toxin action: covalent modification of the guanyl nucleotide-binding protein of the adenylate cyclase system. Proc Natl Acad Sci U S A 75, 2669–2673 (1978). [PubMed: 208069]
6. Cheng SH et al. Phosphorylation of the R domain by cAMP-dependent protein kinase regulates the CFTR chloride channel. Cell 66, 1027–1036 (1991). [PubMed: 1716180]
7. Hewlett EL, Guerrant RL, Evans DJ Jr. & Greenough WB 3rd. Toxins of Vibrio cholerae and Escherichia coli stimulate adenyl cyclase in rat fat cells. Nature 249, 371–373 (1974). [PubMed: 4366779]
8. Winter SE et al. Gut inflammation provides a respiratory electron acceptor for Salmonella. Nature 467, 426–429, doi:10.1038/nature09415 (2010). [PubMed: 20864996]
9. Ritchie JM, Rui H, Bronson RT & Waldor MK Back to the future: studying cholera pathogenesis using infant rabbits. MBio 1, doi:10.1128/mBio.00047-10 (2010).
10. Mandlik A et al. RNA-Seq-based monitoring of infection-linked changes in Vibrio cholerae gene expression. Cell Host Microbe 10, 165–174, doi:10.1016/j.chom.2011.07.007 (2011). [PubMed: 21843873]
11. Levin JZ et al. Comprehensive comparative analysis of strand-specific RNA sequencing methods. Nat Methods 7, 709–715, doi:10.1038/nmeth.1491 (2010). [PubMed: 20711195]
12. Heidelberg JF et al. DNA sequence of both chromosomes of the cholera pathogen Vibrio cholerae. Nature 406, 477–483, doi:10.1038/35020000 (2000). [PubMed: 10952301]
13. Wyckoff EE, Mey AR & Payne SM Iron acquisition in Vibrio cholerae. Biometals 20, 405–416, doi:10.1007/s10534-006-9073-4 (2007). [PubMed: 17216354]
14. Troxell B & Hassan HM Transcriptional regulation by Ferric Uptake Regulator (Fur) in pathogenic bacteria. Front Cell Infect Microbiol 3, 59, doi:10.3389/fcimb.2013.00059 (2013). [PubMed: 24106689]

15. Ganz T & Nemeth E Iron homeostasis in host defence and inflammation. Nat Rev Immunol 15, 500–510, doi:10.1038/nri3863 (2015). [PubMed: 26160612]
16. Chassaing B et al. Fecal lipocalin 2, a sensitive and broadly dynamic non-invasive biomarker for intestinal inflammation. PLoS One 7, e44328, doi:10.1371/journal.pone.0044328 (2012). [PubMed: 22957064]
17. Patnaik BK & G HK. Histopathological Studies on Experimental Cholerae. Br J Exp Pathology (1966).
18. Klose KE The suckling mouse model of cholera. Trends Microbiol 8, 189–191 (2000). [PubMed: 10754579]
19. Henderson DP & Payne SM Vibrio cholerae iron transport systems: roles of heme and siderophore iron transport in virulence and identification of a gene associated with multiple iron transport systems. Infect Immun 62, 5120–5125 (1994). [PubMed: 7927795]
20. Tashima KT, Carroll PA, Rogers MB & Calderwood SB Relative importance of three iron-regulated outer membrane proteins for in vivo growth of Vibrio cholerae. Infect Immun 64, 1756–1761 (1996). [PubMed: 8613388]
21. Cuatrecasas P Cholera toxin-fat cell interaction and the mechanism of activation of the lipolytic response. Biochemistry 12, 3567–3577 (1973). [PubMed: 4731193]
22. Duncan RE, Ahmadian M, Jaworski K, Sarkadi-Nagy E & Sul HS Regulation of lipolysis in adipocytes. Annu Rev Nutr 27, 79–101, doi:10.1146/annurev.nutr.27.061406.093734 (2007). [PubMed: 17313320]
23. Snider RM et al. The effects of cholera toxin on cellular energy metabolism. Toxins (Basel) 2, 632–648, doi:10.3390/toxins2040632 (2010). [PubMed: 22069603]
24. Dirusso CC & Black PN Bacterial long chain fatty acid transport: gateway to a fatty acid-responsive signaling system. J Biol Chem 279, 49563–49566, doi:10.1074/jbc.R400026200 (2004). [PubMed: 15347640]
25. Gillis CC et al. Dysbiosis-Associated Change in Host Metabolism Generates Lactate to Support Salmonella Growth. Cell Host Microbe 23, 54–64 e56, doi:10.1016/j.chom.2017.11.006 (2018). [PubMed: 29276172]
26. Bina J et al. ToxR regulon of Vibrio cholerae and its expression in vibrios shed by cholera patients. Proc Natl Acad Sci U S A 100, 2801–2806, doi:10.1073/pnas.2628026100 (2003). [PubMed: 12601157]
27. Son MS, Megli CJ, Kovacikova G, Qadri F & Taylor RK Characterization of Vibrio cholerae O1 El Tor biotype variant clinical isolates from Bangladesh and Haiti, including a molecular genetic analysis of virulence genes. J Clin Microbiol 49, 3739–3749, doi:10.1128/JCM.01286-11 (2011). [PubMed: 21880975]

REFERENCES (Online-only)

28. Fullner KJ & Mekalanos JJ Genetic characterization of a new type IV-A pilus gene cluster found in both classical and El Tor biotypes of Vibrio cholerae. Infect Immun 67, 1393–1404 (1999). [PubMed: 10024587]
29. Angelichio MJ, Spector J, Waldor MK & Camilli A Vibrio cholerae intestinal population dynamics in the suckling mouse model of infection. Infect Immun 67, 3733–3739 (1999). [PubMed: 10417131]
30. Baselski V, Briggs R & Parker C Intestinal fluid accumulation induced by oral challenge with Vibrio cholerae or cholera toxin in infant mice. Infect Immun 15, 704–712 (1977). [PubMed: 870427]
31. Langmead B & Salzberg SL Fast gapped-read alignment with Bowtie 2. Nat Methods 9, 357–359, doi:10.1038/nmeth.1923 (2012). [PubMed: 22388286]
32. Kearse M et al. Geneious Basic: an integrated and extendable desktop software platform for the organization and analysis of sequence data. Bioinformatics 28, 1647–1649, doi:10.1093/bioinformatics/bts199 (2012). [PubMed: 22543367]

33. Love MI, Huber W & Anders S Moderated estimation of fold change and dispersion for RNA-seq data with DESeq2. Genome Biol 15, 550, doi:10.1186/s13059-014-0550-8 (2014). [PubMed: 25516281]
34. Huang da W, Sherman BT & Lempicki RA Systematic and integrative analysis of large gene lists using DAVID bioinformatics resources. Nat Protoc 4, 44–57, doi:10.1038/nprot.2008.211 (2009). [PubMed: 19131956]
35. Schmittgen TD & Livak KJ Analyzing real-time PCR data by the comparative C(T) method. Nat Protoc 3, 1101–1108 (2008). [PubMed: 18546601]
36. Cameron DE, Urbach JM & Mekalanos JJ A defined transposon mutant library and its use in identifying motility genes in Vibrio cholerae. Proc Natl Acad Sci U S A 105, 8736–8741, doi: 10.1073/pnas.0803281105 (2008). [PubMed: 18574146]
37. Grant SG, Jessee J, Bloom FR & Hanahan D Differential plasmid rescue from transgenic mouse DNAs into Escherichia coli methylation-restriction mutants. Proc Natl Acad Sci U S A 87, 4645–4649 (1990). [PubMed: 2162051]
38. Simon R, Priefer U & Puhler A A broad host range mobilization system for in vivo genetic engineering: transposon mutagenesis in gram negative bacteria. Bio/Technology 1, 784–790 (1983)
39. Miller VL & Mekalanos JJ A novel suicide vector and its use in construction of insertion mutations: osmoregulation of outer membrane proteins and virulence determinants in Vibrio cholerae requires toxR. J Bacteriol 170, 2575–2583 (1988). [PubMed: 2836362]
40. Philippe N, Alcaraz JP, Coursange E, Geiselmann J & Schneider D Improvement of pCVD442, a suicide plasmid for gene allele exchange in bacteria. Plasmid 51, 246–255, doi:10.1016/j.plasmid. 2004.02.003 (2004). [PubMed: 15109831]
41. Wang RF & Kushner SR Construction of versatile low-copy-number vectors for cloning, sequencing and gene expression in Escherichia coli. Gene 100, 195–199 (1991). [PubMed: 2055470]
42. Bishop AL, Patimalla B & Camilli A Vibrio cholerae-induced inflammation in the neonatal mouse cholera model. Infect Immun 82, 2434–2447, doi:10.1128/IAI.00054-14 (2014). [PubMed: 24686062]
43. Godinez I et al. T cells help to amplify inflammatory responses induced by Salmonella enterica serotype Typhimurium in the intestinal mucosa. Infect Immun 76, 2008–2017, doi:10.1128/IAI. 01691-07 (2008). [PubMed: 18347048]

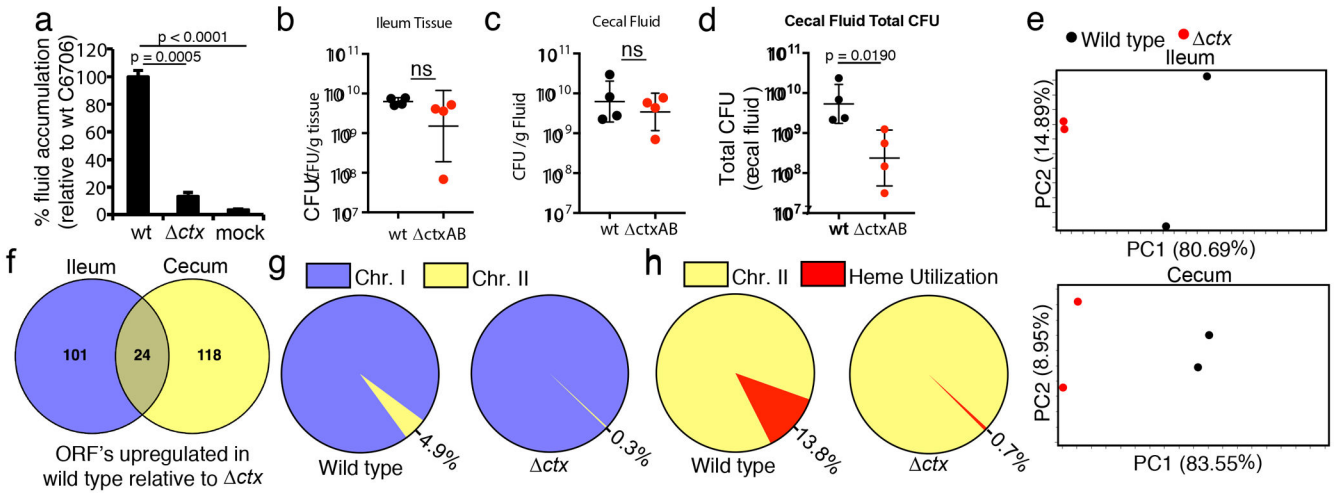

Figure 1. CT induces a unique *Vibrio cholerae* transcriptome signature during infection.

(a-d) Groups of 3-day old New Zealand white rabbits ($N = 4$) were mock-infected or infected intragastrically with 1×10^9 CFU per animal with *V. cholerae* C6706 wild type (wt) or the cholera toxin mutant (Δ*ctx*) and samples were collected one day after infection. (a) The fluid accumulation (FA) ratio in the cecum is expressed as percent of the response observed in animals infected by the wild type strain. The FA ratio of the wild type was compared to the Δ*ctx* mutant or mock using one-way ANOVA ($F(2, 9) = 52.534$, $p < 0.0001$) and post-hoc Sidak's multiple comparisons test. Bars represent percent fluid accumulation relative to wild type ± SE. The CFU/g was determined in the ileum tissue (b), and cecal fluid (c). The total CFU of *V. cholerae* wild type (black circles) or Δ*ctx* mutant (red circles) in the cecal fluid was determined by normalizing the CFU/g by the final weight of the fluid collected from the cecum (d). Error bars represent geometric means ± SD. Bacterial numbers were compared by unpaired two-sided student *t*-test. (e-h) RNA-seq analysis of *Vibrio cholerae* during colonization of the ileum and cecum of infant rabbits (e) PCA plots for RNA-seq data from two biological replicates of *V. cholerae* wild type (black circles) or Δ*ctx* mutant (red circles) collected from the ileum or cecum of infant rabbits ($N = 2$). (f) Venn diagram of genes significantly upregulated in the wild type relative to the Δ*ctx* mutant in the ileum (purple) and cecum (yellow). (g) Percent abundance of raw RNA-seq reads aligned to chromosome I (Chr. I; purple) or chromosome II (Chr. II; yellow) from wild type or the Δ*ctx* mutant in the ileum. (h) Percent abundance of heme utilization genes (VCA0907-VCA0915, VCA0576; red) from raw RNA-seq reads aligned to chromosome II (Chr. II; yellow) from wild type or the Δ*ctx* mutant in the ileum. ns, not statistically significantly different.

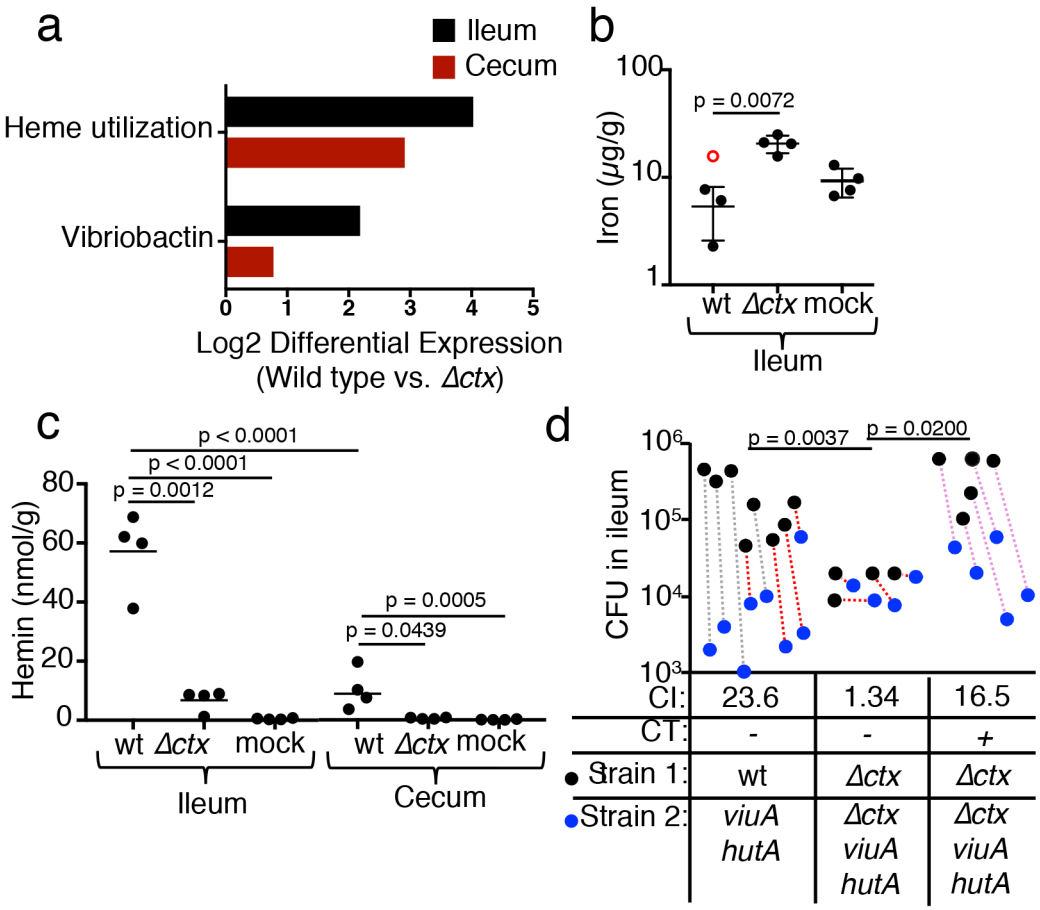

Figure 2. Heme utilization confers a CT-dependent fitness advantage to *Vibrio cholerae*.

(a) RNA-seq analysis of *Vibrio cholerae* heme utilization genes (VCA0907-VCA0915, VCA0576) and vibriobactin genes (VC0200-VC0201, VC2209-VC2211, VC0771-VC0780, VC0475, VCA0227-VCA0230) in the wild type relative to the cholera toxin mutant (Δ*ctx*) in the ileum or cecum. (b) Luminal iron concentrations from the ileum of infant rabbits (*N* = 4) that were mock-infected or infected with the wild type (wt) or the Δ*ctx* mutant. The iron concentrations between type (wt) and the Δ*ctx* mutant were compared by unpaired two-sided student *t*-test. Red dot represents sample from animal containing statistical outlier for *V. cholerae* cholera toxin (*ctxA*) expression. Error bars represent means ± SD. (c) Luminal hemin measurements from the ileum and cecum of infant rabbits (*N* = 4) that were mock-infected or infected with the wild type (wt) or the Δ*ctx* mutant. The wt heme levels in the ileum or cecum were compared to the Δ*ctx* mutant or mock using one-way ANOVA (Ileum: $F(2, 9) = 55.88$, $p < 0.0001$; Cecum: $F(2, 9) = 16.61$, $p = 0.0010$) followed by post-hoc Sidak's multiple comparisons test. The heme levels in the ileum and cecum between groups were compared using two-way ANOVA followed by post-hoc Sidak's multiple comparisons test (see Supplementary Table 7). Black lines show median for individual animals (black circles). (d) Groups of CD-1 mice were infected with a 1:1 mixture of the indicated *V. cholerae* strain mixtures (*N* = 8 for wild type vs *hutA viuA*; *N* = 4 for Δ*ctx* vs Δ*ctx hutA viuA*; *N* = 5 for Δ*ctx* vs Δ*ctx hutA viuA* + CT). Some mice received an oral dose of purified CT mixed into the inoculum. The competitive index (CI; the ratio of strains recovered) was

determined one day after infection. Dotted lines connect strains recovered from the same animal. The CI was compared using one-way ANOVA ($F(2, 14) = 7.634$, $p = 0.0057$) followed by post-hoc Sidak's multiple comparisons test. Different colored lines distinguish animals from different litters. ns, not statistically significantly different.

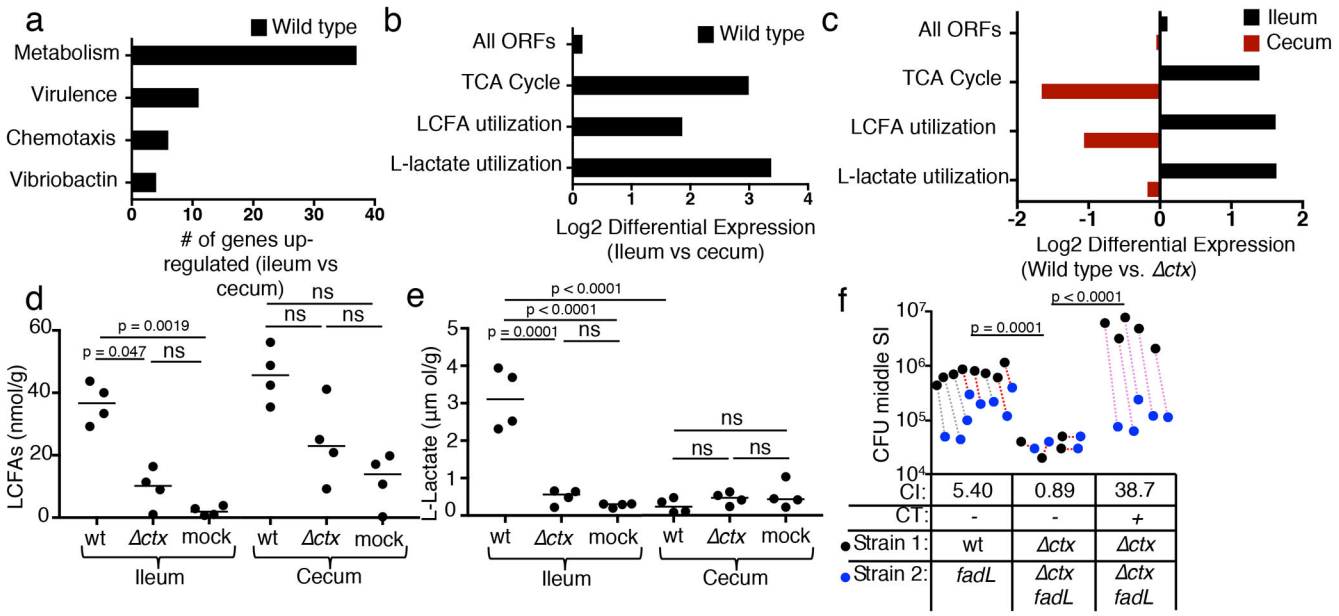

Figure 3. Cholera toxin promotes *Vibrio cholerae* LCFA utilization during infection.

(a) DAVID bioinformatics pathway analysis of RNA-seq data of significantly upregulated pathways in the ileum relative to the cecum. (b) Differential expression of *V. cholerae* genes involved in TCA cycle (VC0432, VC1573, VC2084-VC2092, VC2738), LCFA utilization (VC1043, VC2758, VC2231), and L-Lactate utilization (VCA0983, VCA0984), and all open reading frames (ORFs) of wild type C6706 during colonization of the ileum relative to the cecum. (c) Differential expression of *V. cholerae* genes involved in TCA cycle, LCFA utilization, and L-Lactate utilization, and all ORFs in the wild type relative to the cholera toxin mutant (Δ*ctx*) during colonization of the ileum or cecum. (d) Luminal LCFA measurements (8 carbon chain or greater) from the ileum and cecum of infant rabbits (N = 4) that were mock-infected or infected with the wild type (wt) or the cholera toxin mutant (Δ*ctx*). Black lines show median for individual animals (black circles). The wt LCFA levels in the ileum or cecum were compared to the Δ*ctx* mutant or mock using one-way ANOVA (Ileum: F (2, 9) = 12.69, p = 0.0024; Cecum: F (2, 9) = 2.951, p = 0.1034) followed by post-hoc Sidak's multiple comparisons test. (e) Luminal L-lactate measurements from the ileum and cecum of infant rabbits (N = 4) that were mock-infected or infected with the wild type (wt) or the cholera toxin mutant (Δ*ctx*). Black lines show median for individual animals (black circles). The wt L-Lactate levels in the ileum or cecum were compared to the Δ*ctx* mutant or mock using one-way ANOVA (Ileum: F (2, 9) = 50.98, p < 0.0001; Cecum: F (2, 9) = 1.916, p = 0.2027) followed by post-hoc Sidak's multiple comparisons test. The L-Lactate levels in the ileum and cecum between groups were compared using two-way ANOVA (see Supplementary Table 7) followed by post-hoc Sidak's multiple comparisons test. (f) Groups of CD-1 mice were infected with a 1:1 mixture of the indicated *V. cholerae* strain mixtures (N = 8 for wild type vs *fadL*; N = 4 for Δ*ctx* vs Δ*ctx fadL*; N = 5 for Δ*ctx* vs Δ*ctx fadL* + CT). Some mice received an oral dose of purified CT mixed into the inoculum. The competitive index (CI; the ratio of strains recovered) was determined one day after infection. Dotted lines connect strains recovered from the same animal. The competitive indices between groups were compared using one-way ANOVA (F (2, 14) = 57.98, p <

0.0001) followed by post-hoc Sidak's multiple comparisons test. Different colored lines distinguish animals from different litters. ns, not statistically significantly different.